Total words: 7302

Study on Performance of a Novel Asphalt Mixture Containing Strength and Morphology Controlled Artificial Aggregates

Guangwei Chen[a], Xu Yue[b], Yadong Xie[b], Lin Kong[b], Yue Huang[c], Dongya Ren[a,b,*]

[a] SWJTU-LEEDS Joint School, Southwest Jiaotong University, Chengdu, Sichuan, 610031, China.

[b] School of Civil Engineering, Southwest Jiaotong University, Chengdu, Sichuan, 610031, China.

[c] Institute for Transport Studies, University of Leeds, LS2 9JT, UK.

[*]Corresponding author: Dongya Ren, Tel: +86-18108179712; Email: dongyaren@swjtu.edu.cn

Highlight

- Solid wastes were applied to prepare strength and morphology controlled coarse artificial aggregates by 3D printed mold.
- AAAM exerted superior lightweight property, moisture damage resistance and thermal sensitivity resistance compared to NAAM.
- AAs could eliminate the diversities and differences of aggregate morphology and minimize the variability of testing results.
- Results of paired sample t-tests reported that there was notable effect of AA morphology on the performance of AAAM.

ABSTRACT

The examinations of numerical simulations and investigations on basic behaviors and technical properties of asphalt mixture remained great challenges because of the uncontrolled and varied morphologies of natural coarse aggregates. The traditional ceramsite aggregates were generally associated with weaker skeleton contact and inferior cohesion characteristics because they were porous and spherical. In this study, two kinds of strength and morphology controlled coarse artificial aggregates (AAs) were produced with solid wastes including fly ash and bauxite residues based on 3D printing technology. After sintering, the coarse AAs were applied to prepare three kinds of artificial aggregate asphalt mixtures (AAAMs). The service performance of AAAMs was measured and compared to natural aggregate asphalt mixtures (NAAMs). Coefficient of variation (CV) values and paired sample t-test were applied to evaluate the impact of coarse AAs morphology. The result revealed that AAAMs exhibited superior lightweight characteristic, whose bulk specific gravity decreased by 10% approximately when compared to NAAMs. Except for residual strength ratio (RSR) of RG2-20-L, coarse AAs exerted positive effects on the improvement of moisture damage resistance and thermal sensitivity resistance including rutting resistance and low-temperature cracking resistance. The service performance of AAAMs could meet the technical requirements of specification and construction. CV values of AAAMs were smaller than that of NAAMs, demonstrating that the AAs with identical morphology eliminated the variability of testing results and providing a scientific base for examinations of numerical simulations. Results of paired sample t-tests reported that there was notable effect of AAs morphology on the performance of AAAMs.

Key Words: asphalt mixture; artificial aggregates; aggregate particles morphology; coefficient of variation

1 Introduction

Asphalt mixture contained various gradations of aggregates (more than 90% in weight) and asphalt binder. As the skeleton of asphalt mixture, morphological characteristics of coarse aggregates including angularity, shape and texture exerted the significant difference on basic behaviors and technical properties of asphalt mixture.(Gao et al., 2018; Li et al., 2019; Li et al., 2022b; Wang et al., 2016) The researchers and engineers realized that it was an important research area to establish the relationships between performance of asphalt mixture and morphological characteristics of coarse aggregates.(Ding et al., 2024; Liu, Y. et al., 2017) In the early years, macroscopic mechanical experiments were applied to establish and demonstrate the relationships between the morphological characteristics and performance of asphalt mixture.(Goetz and Herrin, 1954; Meier, 1988; Monismith, 1970) With the development of computer science, numerical simulation models were developed to investigate the significance of morphological characteristics on asphalt mixture.(Hu et al., 2019; Kusumawardani and Wong, 2020; Lei et al., 2024; Li et al., 2024; Liu et al., 2023) Zou et al.(Zou et al., 2023) revealed that the coarse aggregate morphology was crucial to shear strength of asphalt mixture based on 3D discrete element model. Liu et al.(Liu, P. et al., 2017) established the initial relationships between angularities of aggregates and mechanical performance of asphalt mixture by 3D finite element model. However, because of the computer capacity, it was still challengeable to maintain the original morphological characteristics of the aggregates when finite element method or discrete element method was applied to reconstructed. It was also inevitable that the accuracy of the reconstructing models and speed of calculation relied more on the computational capacity as models were characterized by high precision and different sizes.(Jin et al., 2021) Besides, it was worth noting that the error bars of testing results in same tests were obvious, indicating the observable differences of values were greater. Even worse, due to the differences between indoor tests and in-field construction, these tests were less likely to obtain the desired results even the same materials and the same asphalt mixture gradations were practiced.(Xu et al., 2021; Yu et al., 2020; Yu et al., 2019) Therefore, it was reasonable that the standard coarse aggregates with specific morphology were able to minimize these uncertainties and errors that were caused by different conditions and various materials. Nevertheless, the examinations of numerical simulations and investigations on basic behaviors and technical properties of asphalt mixture remained great challenges because of the uncontrolled and random morphologies of natural coarse aggregates. It was also the limitation of theories in the asphalt pavement.

As known, the aggregates used in asphalt mixture were generally natural minerals, which were further processed by crusher into different particle sizes. In the pursuit of promoting a low-carbon concept in road industry, solid wastes including fly ash, coal slag, metal slag were applied to prepare lightweight aggregates, which aimed to explore the feasibility for the replacement of natural aggregates in asphalt mixture.(Andrzejuk et al., 2018; Cho et al., 2023; Deng et al., 2019; Liu et al., 2019; Rodríguez-Fernández et al., 2021; Vila-Cortavitarte et al., 2018) Especially, the utilization of ceramsite aggregates prepared by waste powders had been demonstrated by laboratory experiments and surveys.(Che et al., 2018; Wang et al., 2019; Yuan et al., 2022) This kind of aggregates was generally pelletized and produced by hands or machines, whose fresh particles were further processed during the hardening stages. In addition, AAs prepared by the sintering process were able to achieve better strength and proper volumetric parameters when compared to the cold bonded method.(Priyadharshini et al., 2012) It could be explained by the chemical reaction to develop mullite, which was characterized by high strength and good durability. Nevertheless, the traditional ceramsite aggregates were generally porous and spherical, allowing the liquid binder to be absorbed, thus resulting in weaker skeleton contact and inferior cohesion characteristics.(Min et al., 2022; Xie et al., 2016)

With the evolution of high-precision 3D printing equipment and further investigations on special materials, 3D printing technology had been widely used in various industries to prepare stable and repeatable materials, including construction industry.(Ambrosi and Pumera, 2016; Ramya and Vanapalli, 2016; Sahana and Thampi, 2018; Shahrubudin et al., 2019; Yan et al., 2018) Specifically, acrylonitrile butadiene styrene resin and photosensitive resin were mainly used in 3D printing models with high precision. But these kinds of AAs with specific morphology hardly met the requirements and specification of pavement engineering.(Kim et al., 2023; Yang et al., 2019) Similarly, regarding the effectiveness, precision and performance, it was still impractical that the cement-based materials were applied to prepare AAs by 3D printing technology. Recently, the AAs, prepared by cement-based materials were characterized by inferior mechanical performance and poor volumetric parameters, such as poorer Los Angeles coefficient and higher water absorption.(Li et al., 2022a) The hardening stages were also time-consuming because cement-based material must be further processed to achieve strength development, which was the basic disadvantage for these kinds of materials.

To this end, this study aimed to investigate the feasibility of the asphalt mixture prepared by strength and morphology controlled coarse AAs. Based on 3D printing technology, two kinds of strength and morphology controlled coarse AAs were pelletized by printing mold using fly ash, bauxite residues, bauxite and sintering additives, which were further processed in the sintering furnace to achieve superior mechanical performance and proper volumetric parameters. After the sintering process, the coarse AAs were applied to prepare three kinds of AAAM. Technical properties including aggregate crushing value (ACV), Los Angeles coefficient (LA), polished stone value (PSV), solmdness, adhesiveness and bulk specific gravity (BSG), open porosity (OP) and water absorption (WA) were tested in the previous paper.(Wang et al., 2022) The service performance including lightweight characteristic, Marshall stability, moisture damage resistance, rutting resistance and low-temperature cracking resistance of AAAMs and NAAMs, was compared to analyze the application of asphalt mixture containing strength and morphology controlled coarse AAs. CV values and paired sample t-test were employed to analyze the impact of specific morphology AAs on testing results.

2 Materials and sample preparation

2.1 Artificial aggregate

The raw materials to prepare AAs were waste powders, bauxite and sintering additives, including fly ash and bauxite residues, bauxite, feldspar, MnO_2, talcum-AlF_3 and $BaCO_3$. The properties of the raw materials were shown in Table 1.

The strength development of artificial aggregates referred to the formation of secondary mullite, which could be prepared at the temperature of 1600 ºC. And the mechanisms were explained by four chemical reaction formulas.(Chen, 2018) First, at the temperature of 400-500 ºC, metakaolinte ($Al_2O_3 \cdot 2SiO_2$) could be obtained. As the temperature increased to 900 ºC, Al-Si-Spinel and amorphous $2SiO_2$ developed, after which primary mullite was promoted and then the strength developed. But the strength of primary mullite could not meet the requirements of aggregates used in pavement construction in this case. Continuously, corundum, and amorphous SiO_2 that was derived from metakaolinte, reacted together to produce secondary mullite at the temperature of 1200 ºC. When the sintering temperature continued to increase (about 1600 ºC), the secondary mullite crystals would recombine and larger secondary mullite crystals then developed, whose strength could meet the requirements of aggregates used in pavement construction.

To lower the temperature to prepare artificial aggregates, sintering additives including feldspar, MnO_2, talcum-AlF_3 and $BaCO_3$ were employed into the raw materials. The introduction of feldspar was to effectively control the crystallization process of mullite and the formation of optimal glass phase. MnO_2 was introduced to promote the crystallization of mullite at comparably lower temperature. Also, with the addition of MnO_2, the formation of mullite materials accelerated during the sintering process. Talcum-AlF_3 acted as flux catalyst in the chemical reaction, facilitating the formation of the secondary mullite. To improve acid resistance of artificial aggregates, $BaCO_3$ was employed in the raw materials. The introduction of $BaCO_3$ could promote the formation of byproducts, $Ba_{0.75}Al_{11}O_{17.25}$ and $Ba_{0.956}Mg_{0.912}Al_{10.088}O_{17}$. Both of them were the critical factors to improve the acid resistance of artificial aggregates.

$$Al_2O_3 \cdot 2SiO_2 \cdot 2H_2O(\text{kaolinite}) \xrightarrow{400\text{-}500\,^{\circ}C} Al_2O_3 \cdot 2SiO_2(\text{metakaolinte}) + 2H_2O$$

$$2(Al_2O_3 \cdot SiO_2)(\text{metakaolinite}) \xrightarrow{-900\,^{\circ}C} Si_3Al_4O_{12}(\text{Al-Si-Spinel}) + 2SiO_2(\text{amorphous})$$

$$3Si_3Al_4O_{12}(\text{Al-Si-Spinel}) \xrightarrow{>1050\,^{\circ}C} 2(3Al_2O_3 \cdot SiO_2)(\text{mullite}) + 5SiO_2(\text{amorphous})$$

$$3Al_2O_3(\text{corundum}) + 2SiO_2 \xrightarrow{1100\text{-}1450\,^{\circ}C} (3Al_2O_3 \cdot 2SiO_2)(\text{secondary mullite})$$

Table 1 Chemical components (wt.%) of materials and sintering additives.

Materials	SiO_2	Al_2O_3	Fe_2O_3	CaO	Other components	L.O.I	Density
Fly ash	53.97	31.15	4.16	4.01	6.69	1.62	2.15
Bauxite	18.79	72.98	2.51	-	5.45	0.91	3.22
Bauxite residues	8.75	14.59	18.88	25.09	8.67	22.02	2.87
Sintering additives							
Feldspar	69.15	15.15	0.71	0.56	13.78	0.03	2.56
Talcum	40.11	0.26	0.21	8.31	33.20	33.18	2.73
MnO_2					Purity >99		5.02
AlF_3					Purity >99		1.91
$BaCO_3$					Purity >99		4.43

Response surface design algorithm (RSD) was employed to investigate the effects among sintering additives and then to obtain the desired content of raw materials. As coarse aggregates were mainly subjected to vehicle load, compressive strength was the responses in the RSD algorithm. According to the 3D contour map in Fig. 1a, there was the negative effect between feldspar and MnO_2, suggesting that the proportion of feldspar should be limited. Fig. 1b depicted a barely notable impact between MnO_2 and talcum-AlF_3, which was similar to the following results of feldspar and Talcum-AlF_3 in Fig. 1c. Therefore, according to RSD algorithm, reference group(RG) was 38.75% fly ash, 38.75% bauxite, 5.5% feldspar, 8.5% MnO_2, 7.5% talcum-AlF_3 and 1% $BaCO_3$.at 1200 ºC. Also, one-sixth of RG mixing powders was replaced with bauxite residues (RG2). The specific procedures could be found in previous study.(Wang et al., 2022)

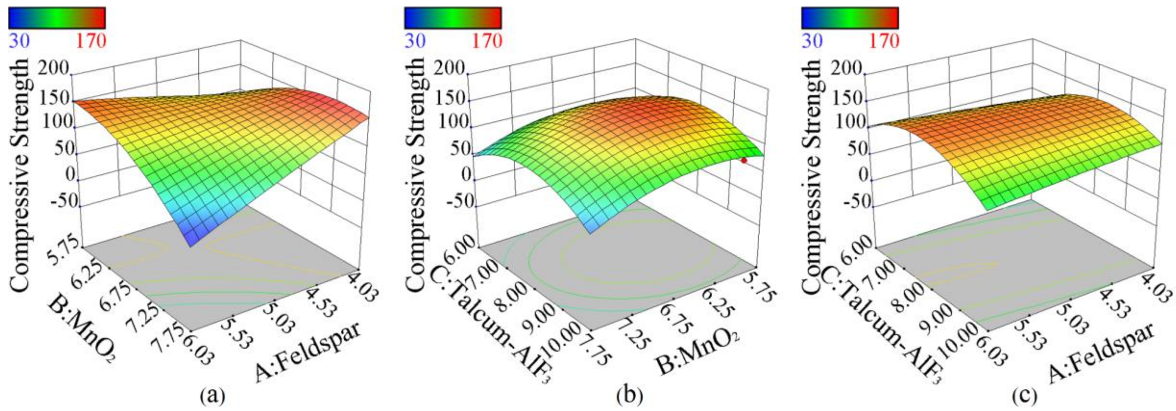

Fig. 1. Effects among sintering additives: (a) feldspar and MnO_2; (b) MnO_2 and talcum-AlF_3; (c) feldspar and talcum-AlF_3.

Computed tomography technology(CT) was applied to reconstruct the 3D digital models of natural aggregates with high accuracy but without destruction. After reconstruction of natural aggregates, the digital mold could be designed by 3D Builder based on the Boolean operation and then be printed based on 3D printing technology. The processes to reconstruct the natural aggregate models and to print mold were summarized in Fig. 2. The details could also be found in previous study.(Wang et al., 2022)

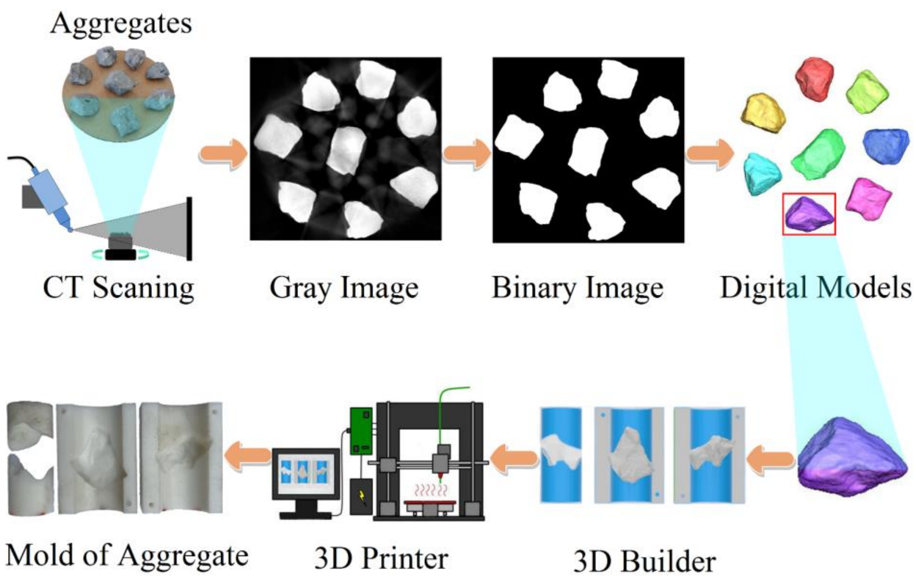

Fig. 2. The processes to reconstruct the natural aggregate models and to print mold.

Fig. 3 illustrated the main steps that the printing mold was employed to prepare the fresh AAs with specific morphology. The optimal proportions and sintering temperature were provided based on RSD algorithm. After sintering, the properties of sintered AAs including ACV, LA, PSV, solmdness, adhesiveness and the volumetric parameters were investigated, which were also presented in Table 2. Specifically, the further information to produce strength and morphology controlled AAs could be found in previous study.(Wang et al., 2022)

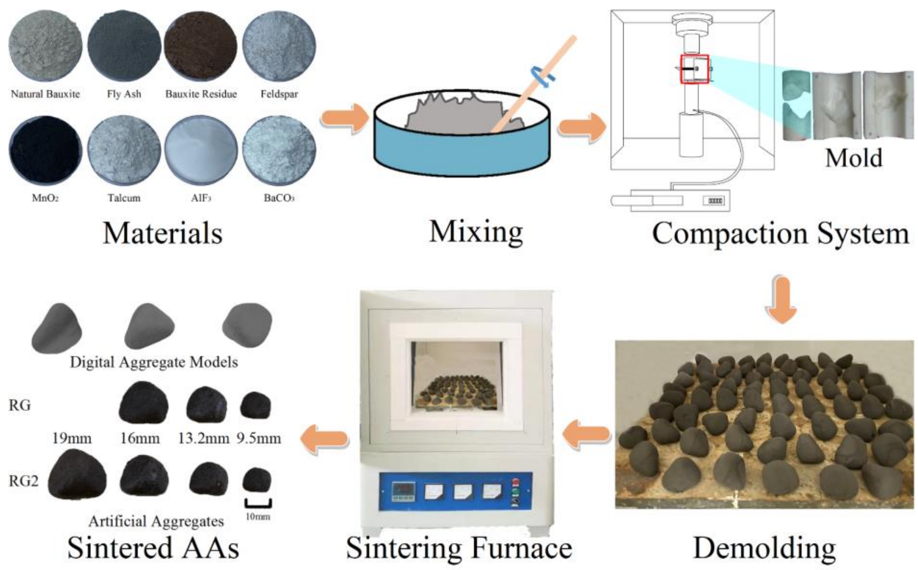

Fig. 3. Main steps to prepare sintered AAs with specific morphology and different sizes.

Table 2 Technical properties of artificial aggregates.

Properties	Unit	RG	RG2	Standard (Wearing layer)	Standard (Other layers)
ACV	%	8.9	14.4	≤20	≤22
LA	%	7.7	17.5	≤18	≤28
PSV	-	45	43	≥42	/
Solmdness	%	2.4	3.1	≤12	≤12
Adhesiveness	-	5	5	5	4
BSG	-	2.41	2.39	-	-
OP	%	0.84	7.13	-	-
WA	%	0.35	2.86	≤2.0	≤3.0

2.2 Natural aggregate

Fig. 4 depicted the aggregates that were applied for six kinds of asphalt mixture in this paper. The natural aggregates used in this study were diabase, granite and limestone, respectively. Specifically, the diabase was provided by Guigang highway mining Co., Ltd. The granite was produced by Gaozhou xinde mining Co., Ltd. The limestone was obtained from Huarun Quarry. The properties of the coarse aggregates and fine aggregates were shown in Table 3 and Table 4, respectively.

Fig. 4. Aggregates applied for six kinds of asphalt mixture.

Table 3 Technical properties of coarse aggregates.

Properties	Unit	Diabase	Granite	Limestone	Standard (Wearing layer)	Standard (Other layers)
ACV	%	8.3	16.3	17.7	≤20	≤22
LA	%	11.5	23.0	21.1	≤18	≤28
PSV	-	44	42	43	≥42	/
Solmdness	%	2.2	3.3	2.6	≤12	≤12
Adhesiveness	-	5	4	4	5	4
BSG	-	2.88	2.70	2.64	-	-
OP	%	2.27	1.03	5.17	-	-
WA	%	0.43	0.42	0.29	≤2.0	≤3.0

Table 4 Technical properties of fine aggregates.

Properties	Unit	Diabase	Limestone	Granite	Standard
Apparent specific gravity	-	2.74	2.77	2.73	≥2.50
Sand equivalent value	%	70	71	76	≥60
Methylene blue value	g/kg	2.0	0.9	1.9	≤25
Angularity	s	38.8	38.6	35.0	≥30

2.3 Asphalt

The styrene-butadiene-styrene (SBS) modified asphalt, whose PG grading was 76-22, was chosen from Dongguan Taihe asphalt Co., Ltd. And the properties were shown in Table 5.

Table 5 Properties of SBS modified asphalt.

Properties	Unit	SBS
Penetration	0.1mm	56
Softening point	ºC	87.0
Ductility	cm	32
Rotational viscosity (135 ºC)	Pa·s	2.28
Critical temperature ($G^*/\sin\delta$=1.0 kPa)	ºC	88
Critical temperature ($G^*/\sin\delta$=2.0 kPa)	ºC	76

2.4 Asphalt mixture

Marshall design principle was employed to determine the optimal asphalt content (OAC). In this study, three kinds of NAAMs were prepared, which were the control groups. And three kinds of AAAMs were prepared, whose natural coarse aggregates were replaced with coarse AAs. The asphalt mixture gradation curves including AC16-D prepared by diabase, AC20-G prepared by granite and AC20-L prepared by limestone, were shown in Fig. 5. The OACs of three kinds NAAMs were determined as 4.7%, 4.5% and 4.4%, respectively. The properties of asphalt mixture were presented in Table 6.

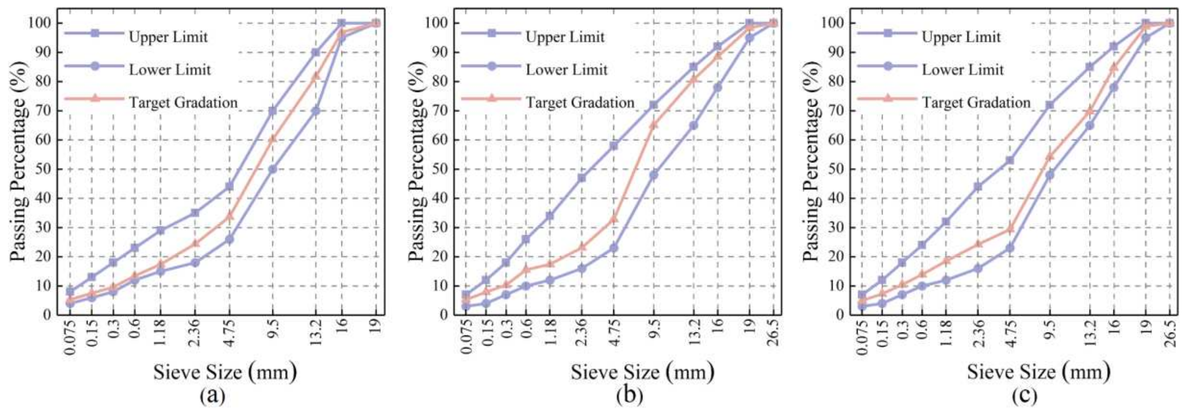

Fig. 5. Asphalt mixture gradation curve: (a) AC16-D; (b) AC20-G; (c) AC20-L.

Table 6 Test results of asphalt mixture based on Marshall design principle.

Properties	Unit	AC16-D	AC20-G	AC20-L
OAC	%	4.7	4.5	4.4
Bulk density of bituminous mixtures	-	2.549	2.432	2.481
Theoretical maximum specific gravity of bituminous mixtures	-	2.661	2.544	2.590
VV	%	4.2	4.4	4.2
VMA	%	14.1	13.3	13.5
VFA	%	70.2	67.0	68.7
Marshall stability	kN	12.95	11.12	12.64
Flow value	mm	3.21	3.09	3.15

2.5 Sample preparation

According to the results of Marshall design principle, six kinds of testing specimens were prepared to investigate the workability and service performance. Specifically, cylindrical specimens were prepared for Marshall test and moisture damage resistance test, whose dimensions were 101.6mm in diameter and 63.5mm in height, respectively. Asphalt mixture slabs were prepared by segmented roller compactor for high temperature performance test, whose dimensions were 300mm in length, 300mm in width and 50mm in height, respectively. Beam-shape specimens were extracted from asphalt mixture slabs for low-temperature cracking resistance test, whose dimensions were 250mm in length, 30mm in width and 35mm in height, respectively. Table 7 presented the details of six kinds of asphalt mixture.

Table 7 Details of six kinds of asphalt mixture.

Mixture label	Description	Note
AC16-D	Asphalt mixture contained natural coarse aggregates and natural fine aggregates	D referred to diabase
RG-16-D	Asphalt mixture contained coarse AAs (natural coarse aggregates with the size of 16mm, 13.2mm and 9.5mm were replaced with the same size of coarse AAs) and natural fine aggregates.	
AC20-G	Asphalt mixture contained natural coarse aggregates and natural fine aggregates	G referred to granite
RG2-20-G	Asphalt mixture contained coarse AAs (natural coarse aggregates with the size of 16mm, 13.2mm and 9.5mm were replaced with the same size of coarse AAs) and natural fine aggregates.	
AC20-L	Asphalt mixture contained natural coarse aggregates and natural fine aggregates	L referred to limestone
RG2-20-L	Asphalt mixture contained coarse AAs (natural coarse aggregates with the size of 16mm, 13.2mm and 9.5mm were replaced with the same size of coarse AAs) and natural fine aggregates.	

3 Testing program

3.1 Marshall test

Marshall stability referred to the maximum value when the failure of the specimen occurred. Meanwhile, the amount of the movement referred to flow value. In this study, Marshall test (JTG E20-2011 T0709-2011) was carried out and the RSR was applied to evaluate the moisture damage resistance of asphalt mixture. For six kinds of asphalt mixture, four replicating tests were performed and the results of each specimen were recorded. The service performance program of asphalt mixture was summarized in Fig. 6.

3.2 Moisture damage resistance test

Moisture damage was a common issue that obviously deteriorated the service life of the asphalt pavement. It could be explained by the fact that the asphalt mixture was continuously swelled and deformed by water as the consequence of freeze-thaw cycles, leading to the cracks development and propagation. And the repeated process deteriorated the mechanical performance and reduced the service life of the asphalt pavement. Indirect tensile strength test (JTG E20-2011 T0729-2011) was used to reveal the moisture damage resistance of asphalt mixture before and after freeze-thaw process. The first step was to put the specimens into the vacuum chamber for 15 minutes, achieving vacuum saturation. Then the saturated specimens were processed by the freeze-thaw cycle including a -18 ºC, 16h freezing step and a 60 ºC, 24h thawing step. The final step was that all the specimens were soaked into waster at 25 ºC for 2h. The indirect tensile strength ratio (ITSR) was employed to assess the moisture damage resistance of asphalt mixture. For six kinds of asphalt mixture, four replicating tests were performed and the results of each specimen were recorded. The service performance program of asphalt mixture was summarized in Fig. 6.

3.3 Rutting resistance test

Rutting mainly attributed to the cumulative plastic deformation of asphalt pavement at high temperature, which basically occurred on the driving path. When subjected to the repeated vehicle load in summer, the void inside asphalt pavement became lower and then denser, thus leading to the formation of rutting. The loading wheel tracking test (JTG E20-2011 T0719-2011) was applied to estimate the rutting resistance performance of asphalt mixture. The compacted slabs were first placed into the 60 ºC air bath chamber for 6h, after which the specimens were subjected to the single rubber wheel under 0.7 MPa for 1h. The rut depth at final 15 minutes, which was also represented by dynamic stability, was used to reveal the rutting resistance of asphalt mixture. For six kinds of asphalt mixture, three replicating tests were performed and the results of each specimen were recorded. The service performance program of asphalt mixture was summarized in Fig. 6.

3.4 Low-temperature cracking resistance test

When the temperature declined suddenly, there was the temperature gradient inside the asphalt pavement. The temperature of the pavement surface was lower that the internal one. The temperature stress developed and accumulated as the asphalt mixture shrank. When the stress was greater than the ultimate strength of asphalt mixture, the cracks occurred and then expanded rapidly. The low-temperature bending test (JTG E20-2011 T0715-2011) was conducted to reveal the low-temperature cracking resistance of asphalt mixture. The beam-shape specimens were extracted from asphalt mixture slabs, followed by placing into the -10 ºC air bath chamber for 6h. The amount of deformation of the specimen when loading to failure was expressed as the limiting flexural strain, which was employed to measure the low-temperature cracking resistance of asphalt mixture. For six kinds of asphalt mixture, four replicating tests were performed and the results of each specimen were recorded. The service performance program of asphalt mixture was summarized in Fig. 6.

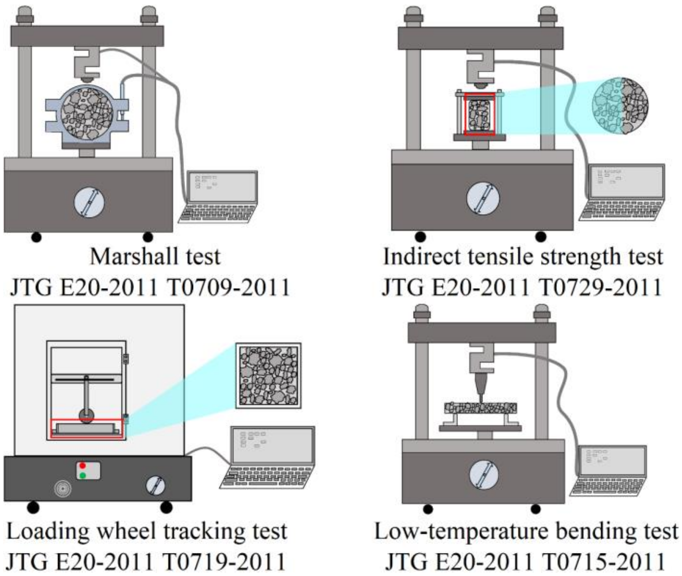

Fig. 6. Service performance programs of asphalt mixture.

3.5 Coefficient of variation and paired sample t-test

The CV value was to measure and compare the variation of a group of numbers, which had been widely used as a result of precision and reproducibility of data in medical and biological science. It could eliminate the interference of the testing results from other factors, providing the assessment for determining the variability of several testing results in the same test. In this study, CV value was used to evaluate the variability of each result when performing the same test. The CV value was desired to satisfy the following equation.

$$\mathrm{CV} = \frac{\sigma}{\mu}$$

where CV was coefficient of variation (in %); σ was the standard deviation of testing result in the same program, μ was the mean of testing result in the same program.

There were three kinds of t-tests in statistical method, independent samples t-test, one sample t-test and paired sample t-test. Generally, t-tests were widely used to determine the differences of variables. Particularly, the paired sample t-test was basically applied to investigate the difference of paired groups, which was assessed and compared by t-value and p-value between paired variables. When the p-value was less than or equal to α-value ($p \leq 0.05$), the paired variables exerted the notable differences and the robust correlations. The t-value was computed as followed.

$$t = \frac{\overline{D}}{\frac{S_d}{\sqrt{n}}}$$

Where $\overline{D}$ was the mean of paired testing results in the same program; S_d was the standard deviation of paired testing result in the same program; n was the number of pairs.

4 Results and discussion

4.1 Lightweight characteristic

The asphalt mixture containing AAs exerted the superior significance on the lightweight characteristic when compared to that containing natural aggregates. As shown in Fig. 7a, the BSGs of AAAMs were in the range between 2.264 and 2.270 while those of NAAMs were in the range between 2.432 and 2.549. It could be concluded that the BSGs of all AAAMs were smaller than those of NAAMs. Specifically, the BSG of RG-16-D decreased from 2.549 to 2.264 when the natural coarse aggregates were replaced with RG. It could be observed in Fig. 7c that there were lots of porosities inside RG. As depicted in Fig. 7b, RG was characterized by lower WA, indicating that this kind of porosities were inner porosities. It could also be observed form the Fig. 7c that that liquid binder would not be absorbed by RG. And this value variation trends of the other asphalt mixture (RG2-20-G and RG2-20-L) containing AAs were similar to RG-16-D. Generally, the lightweight characteristic was a positive advantage in steel bridge deck pavement, for which the asphalt mixture with RG was much lighter, reducing the dead load or improving service life by increasing the thickness. Therefore, this kind of AAs was able to achieve high strength but lightweight properties for special pavements.

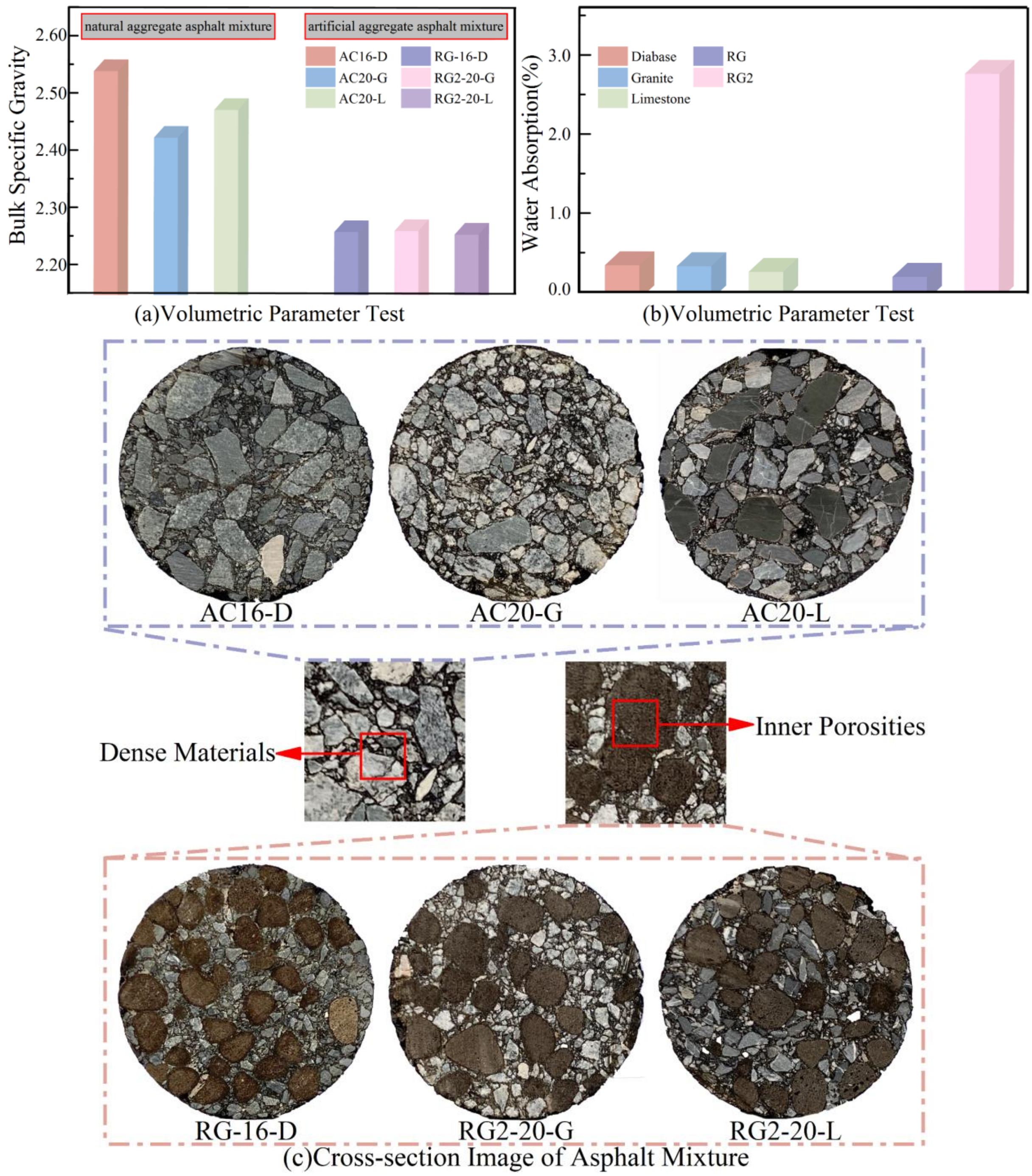

Fig. 7. Lightweight characteristic of asphalt mixture: (a) bulk specific gravity of asphalt mixture; (b) water absorption of aggregates; (c) cross-section image of asphalt mixture.

4.2 Marshall stability and residual strength ratio

The Marshall stability of all kinds of asphalt mixture could meet the requirements of specification and construction, revealing the great moisture damage resistance under water action and the condition at the temperature of 60 ºC. As indicated in Fig. 8a, the RSRs were larger than 85%. And as shown in Fig. 8b, the standard Marshall stabilities of all kinds of asphalt mixture were higher than 8 kN, which were the minimum threshold values in the specification, respectively. So the addition of AAs would not have the negative impact on the performance of moisture damage resistance. Fig. 8a depicted that the RSR of RG2-20-G significantly increased as RG2 was introduced. It could be explained that granite aggregates were acid, whose adhesiveness grade was only 4. When water moved into the asphalt mixture, it was more likely to loose and drop the particles under the water action and repeated vehicle load if adhesiveness grade was much lower. As depicted in Fig. 8b and Fig. 8c, the immersion Marshall stability of RG2-20-L was still comparable to the standard Marshall stability of AC20-L though the RSR of RG2-20-L decreased. Therefore, the introduction of AAs would not deteriorate the properties of moisture damage resistance.

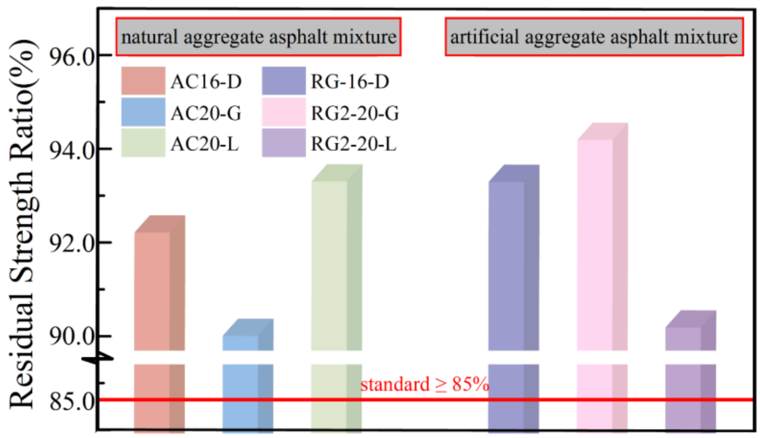

(a)Marshall Test

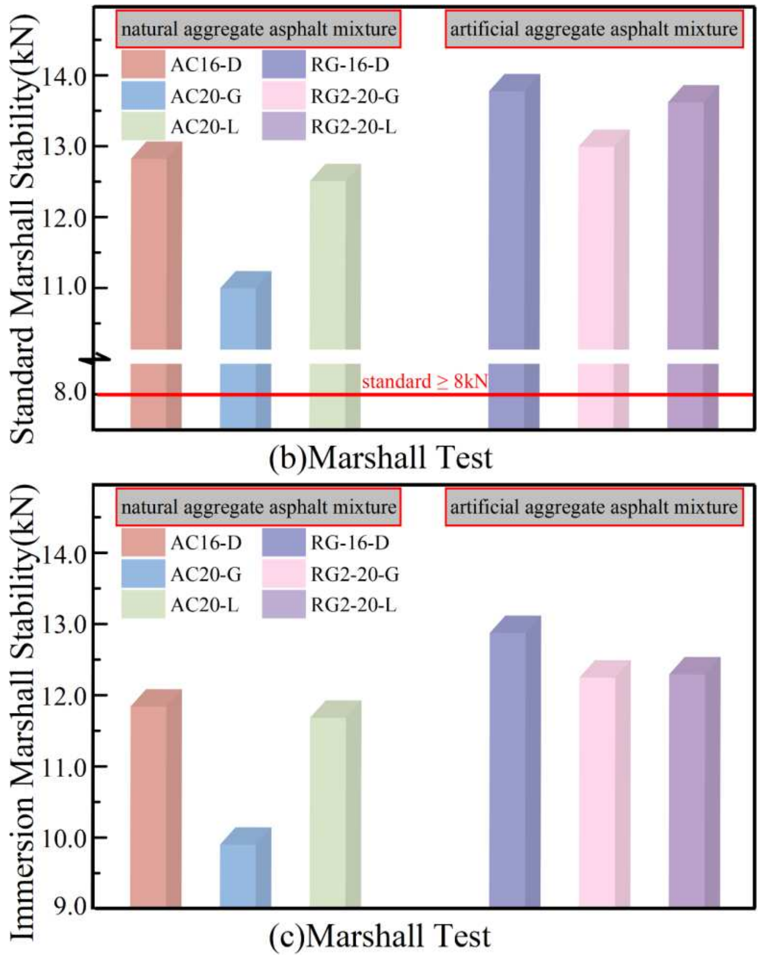

Fig. 8. Marshall test: (a) residual strength ratio; (b) standard Marshall stability; (c) immersion Marshall stability.

4.3 Moisture damage resistance

As presented in Fig. 9a, ITSRs of all kinds of asphalt mixture were greater than 80%, meeting the requirements of specification and construction, and revealing the superior moisture damage resistance under freeze-thaw cycles. As RG-16-D and RG2-20-G showed the obvious enhancement in ITSRs, the addition of RG or RG2 would not decrease the ITSRs of asphalt mixture but actually increase that. The ITSR of RG-16-D increased from 85.5% to 88.5% and that of RG2-20-G raised from 87.3% to 90.9% when replacing natural aggregates with RG and RG2, respectively. Also, RG2-20-G and RG2-20-L exhibited the maximum ITSRs among all asphalt mixture, whose values were all greater than 90%, implying the non-negligible effect of RG2 on moisture damage resistance of asphalt mixture. As indicated in Fig. 9b and Fig. 9c, it was notable that the indirect tensile strengths (ITSs) of AAAMs were all greater than 1 MPa before and after freeze-thaw cycles. However, the ITSs of NAAMs were all less than 1 MPa after freeze-thaw cycles, demonstrating that the introduction of RG and RG2 had positive impact on moisture damage resistance of AAAMs. And the largest indirect tensile strength before and after freeze-thaw cycles belonged to RG-16-D.

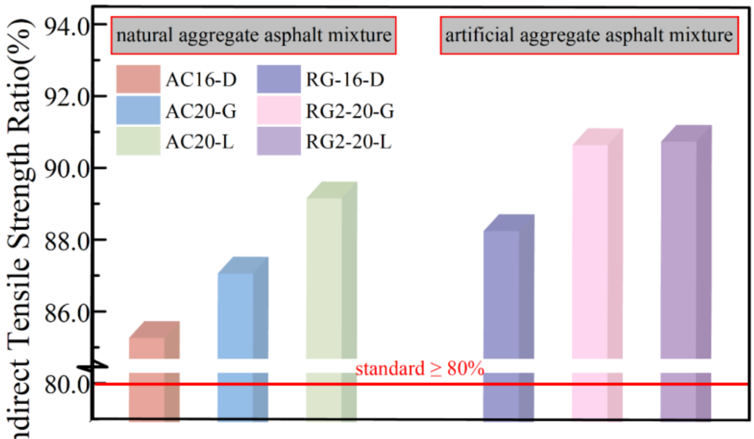

(a)Indirect Tensile Strength Test

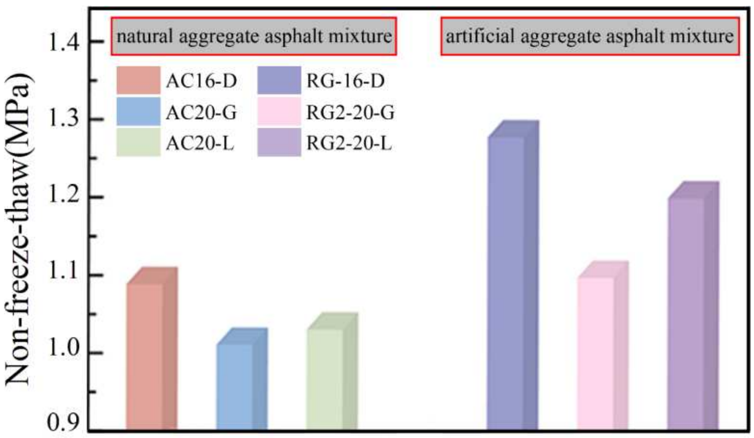

(b)Indirect Tensile Strength Test

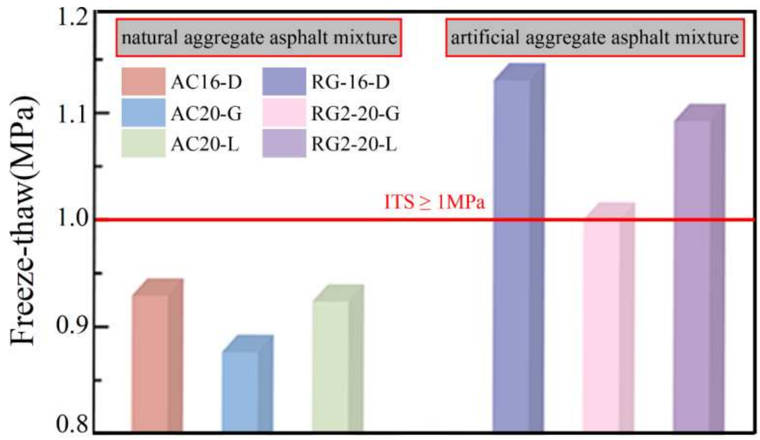

(c)Indirect Tensile Strength Test

Fig. 9. Indirect tensile strength test: (a) indirect tensile strength ratio; (b) non-freeze-thaw group; (c) freeze-thaw group.

4.4 Rutting resistance

The dynamic stabilities of all kinds of asphalt mixture were all higher than 3000 cycle/mm, which was the minimum threshold value required by specification and construction, demonstrating the outstanding ability to resist rutting failure under repeated vehicle load. It was clear that the introduction of RG or RG2 would not deteriorate the dynamic stability of AAAMs but actually enhance that. As illustrated in Fig. 10, the dynamic stability of RG-16-D rose from 9537 cycle/mm to 11475 cycle/mm, which was the desired improvement among all asphalt mixture. It could also be found that the dynamic stability of RG2-20-G increased by approximately 1300 cycle/mm, whose improvement was similar to RG2-20-L. In addition, after the natural coarse aggregates were replaced with RG2, the dynamic stabilities of RG2-20-G and RG2-20-L were comparable to AC16-D, indicating that the noticeable impact of RG2 on rutting resistance of asphalt mixture. Typically, the middle layer was required to exhibit excellent rutting resistance performance to minimize cumulative permanent distress when subjected to repeated vehicle load at high temperature. In this case, the results of loading wheel tracking test implied that the RG2-20-G and RG2-20-L were able to be applied for middle layer of asphalt pavement construction, providing suitable service performance at high temperature.

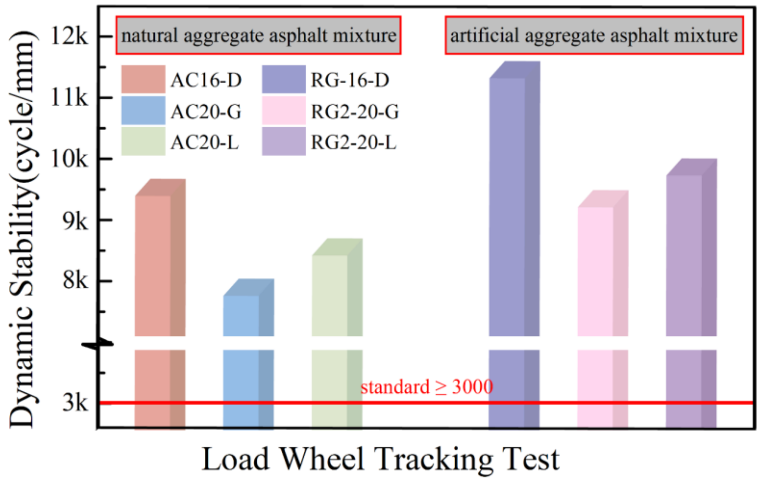

Fig. 10. Loading wheel tracking test.

4.5 Low-temperature cracking resistance

The maximum tensile strains of all kinds of asphalt mixture were all higher than 2500 με, which was the minimum threshold value required by specification and construction, implying the suitable ability to resist cracking failure at low temperature. It was also suggested that the incorporation of RG or RG2 exhibited the positive influence on cracking resistance behavior of AAAM. As seen in Fig. 11, the maximum tensile strain of RG2-20-L increased from 2741 με to 3431 με, which was the biggest improvement among all asphalt mixture. It was worth noting that the maximum tensile strain of RG-16-D was higher than AC20-G and AC20-L when natural coarse aggregates were replaced with RG. In addition, it could be observed that the maximum tensile strain of RG-16-D increased by roughly 500 με, whose improvement was comparable to RG2-20-G. Basically, the bottom layer was required to present great cracking resistance performance in order to limit shrinkage failure at low temperature. According to the maximum tensile strain results, AAAMs were able to be applied for bottom layer of asphalt pavement construction, providing suitable service performance at low temperature.

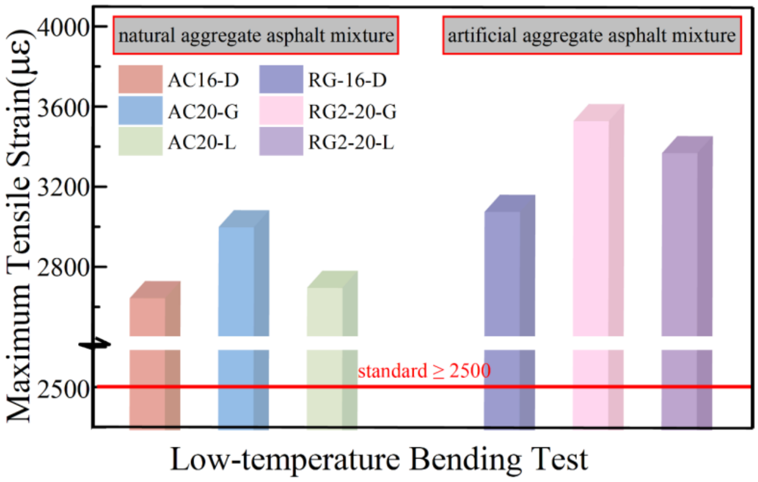

Fig. 11. The low-temperature bending test.

4.6 Coefficient of variation and paired sample t-test

CV values could quantitatively assess and determine the variability of several testing results in the same test. Table 8 summarized the CV values of Marshall stability (standard and immersion), indirect tensile strength (freeze-thaw group and non-freeze-thaw group) and maximum tensile strain in the same test. As shown in Table 8, the CV value of AC16-D was higher than that of RG-16-D in standard Marshall test, indicating that the introduction of RG could significantly minimize the variability of testing results. And the CV values of RG2-20-G and RG2-20-L exhibited the similar variation trend in standard Marshall test. Firstly, every natural aggregate was characterized by random morphology and uncontrollable property because natural rock was further processed by crusher into different particle sizes after explosion and extraction. In terms of AAs, they were prepared by 3D printing mold, whose morphology was almost identical. And the differences of mechanical performance, chemical properties and volumetric parameters among different AAs could also be neglected. When considering the types of aggregates, it could be observed that the improvement of granite and limestone was more effective. The granite aggregates were acid, whose adhesiveness between asphalt and aggregate was much poor. Further, there were much cracks inside the limestone, where the $CaCO_3$ crystals were developed in the cracks. Both factors thus led to higher CV values of AC20-G and AC20-L. It could also be observed that the CV values of AAAMs shared the similar trends in immersion Marshall stability, indirect tensile strength (freeze-thaw group and non-freeze-thaw group) and maximum tensile strain. Therefore, it could be concluded that the CV values of AAAMs were smaller than NAAMs because of the replacement of natural aggregates with AAs.

Table 8 The CV values of several testing results in the same test.

Test	Type	Mean	CV(%)
Standard Marshall stability (0.5h)	AC16-D	12.95	3.05
	RG-16-D	13.91	1.42
	AC20-G	11.12	3.42
	RG2-20-G	13.13	1.37
	AC20-L	12.64	5.04
	RG2-20-L	13.76	1.96
Immersion Marshall stability (48h)	AC16-D	11.97	3.41
	RG-16-D	13.01	1.33
	AC20-G	10.03	3.43
	RG2-20-G	12.39	1.60
	AC20-L	11.82	3.34
	RG2-20-L	12.44	1.03
Indirect tensile strength (non-freeze-thaw group)	AC16-D	1.10	8.03
	RG-16-D	1.29	5.66
	AC20-G	1.02	6.99
	RG2-20-G	1.11	3.75
	AC20-L	1.04	10.86

	RG2-20-L	1.21	4.23
Indirect tensile strength (freeze-thaw group)	AC16-D	0.94	7.04
	RG-16-D	1.14	3.43
	AC20-G	0.89	12.57
	RG2-20-G	1.01	3.88
	AC20-L	0.93	11.79
	RG2-20-L	1.10	3.17
Maximum tensile strain	AC16-D	2687	8.05
	RG-16-D	3122	4.94
	AC20-G	3042	12.92
	RG2-20-G	3576	2.20
	AC20-L	2741	8.20
	RG2-20-L	3417	2.68

To evaluate effects of AAs with specific morphology on the performance, paired sample t-test was employed in this study. Firstly, it was assumed that there was no effect of AAs with specific morphology on the performance. Further, when the p-value was less than or equal to α-value ($p \leq 0.05$), the null hypothesis could be rejected. So it could be concluded that the AAs with specific morphology exerted notable effect on the performance of asphalt mixture. The widely used confidence interval of difference were the 90%, 95%, 99%. In this study, the confidence intervals of difference were 95%. Table 9 listed the paired sample t-test results of Marshall stability (standard and immersion), indirect tensile strength (freeze-thaw group and non-freeze-thaw group) and maximum tensile strain in the same test. According to Table 9, the p-value of the paired samples, AC16-D and RG-16-D in Standard Marshall test was 0.01558, which was smaller than the α-value ($p \leq 0.05$). So the paired sample t-test results revealed that there was notable effect between two sets of analyzed data, indicating that the introduction of AAs with specific morphology had a significant impact on the performance of asphalt mixture. It could also be observed that the p-values of other paired samples exhibited the similar trends in the Marshall stability (standard and immersion), indirect tensile strength (freeze-thaw group and non-freeze-thaw group) and maximum tensile strain. Therefore, it could be concluded that the AAs with specific morphology exerted notable effect on the performance of asphalt mixture.

Table 9 Paired sample t-test results in the same test.

Test	Type	95% Confidence Interval of the Difference		Pr>| t |
		Lower	Upper	
Standard Marshall stability (0.5h)	AC16-D RG-16-D	-1.64589	-0.28411	0.01558
	AC20-G RG2-20-G	-2.67738	-1.33762	0.00212
	AC20-L RG2-20-L	-2.14827	-0.08673	0.03291
Immersion Marshall stability (48h)	AC16-D RG-16-D	-1.76188	-0.32812	0.01471
	AC20-G RG2-20-G	-2.91837	-1.80163	0.00078
	AC20-L RG2-20-L	-1.40601	0.03101	0.03982
Indirect tensile strength (non-freeze-thaw group)	AC16-D RG-16-D	-0.43957	0.05957	0.03433
	AC20-G RG2-20-G	-0.21379	0.00879	0.01025
	AC20-L RG2-20-L	-0.41957	0.07957	0.04115
Indirect tensile strength (freeze-thaw group)	AC16-D RG-16-D	-0.35422	-0.05078	0.00792
	AC20-G RG2-20-G	-0.30526	0.05526	0.00285
	AC20-L RG2-20-L	-0.36139	0.02139	0.02062
Maximum tensile strain	AC16-D RG-16-D	-641.49019	-228.50981	0.0029
	AC20-G RG2-20-G	-929.44742	-137.88591	0.01791
	AC20-L RG2-20-L	-891.75155	-461.91511	0.00045

5 Conclusions

Based on 3D printing technology, two kinds of strength and morphology controlled coarse

AAs (RG and RG2) were prepared by printing mold using fly ash, bauxite residues, bauxite and sintering additives in this study. After the sintering process, the coarse AAs were applied to prepare three kinds of AAAM, namely RG-16-D, RG2-20-G and RG2-20-L. The service performance including lightweight characteristic, Marshall stability, moisture damage resistance, rutting resistance and low-temperature cracking resistance of AAAM and NAAM, was compared. CV values and paired sample t-test were employed to analyze the impact of specific AAs on testing results. According to results, the following conclusions could be drawn.

1. The BSGs of AAAMs were in the range between 2.264 and 2.270 while those of NAAMs were in the range between 2.432 and 2.549. Because there were lots of porosities inside AAs and the AAs were also characterized by lower WA, the liquid binder would not be absorbed by AAs. So the BSGs of all AAAMs were smaller than those of NAAMs. Basically, the BSGs of AAAMs decreased by 10% approximately when compared to NAAMs.
2. Three kinds of AAAMs achieved the required moisture damage resistance, whose RSRs and ITSRs all met the requirements of specification and construction. Except for the RSR of RG2-20-L, RG and RG2 exhibited the positive impact on the improvement of moisture damage resistance.
3. The incorporation of AAs enhanced the thermal sensitivity resistance of three kinds of AAAMs, minimizing cumulative permanent deformation at high temperature and limiting shrinkage failure at low temperature. They could be applied for middle layer and bottom layer because of the excellent rutting resistance and cracking resistance, respectively.
4. Compared to NAAMs, the CV values of AAAMs in Marshall stability (standard and

immersion), indirect tensile strength (freeze-thaw group and non-freeze-thaw group) and maximum tensile strain in the same test were all smaller. The introduction of AAs prepared by 3D printing mold was able to eliminate the diversities of aggregate morphology, reduce the differences in aggregate properties and then minimize the variability of testing results.

5. According to the paired sample t-test results, the p-values of paired samples were all smaller than the α-values. The introduction of AAs with specific morphology had a significant impact on the performance of AAAMs, demonstrating that there was notable effect of AAs morphology on the performance of AAAMs.

In this paper, two kinds of strength and morphology controlled coarse AAs were prepared using solid wastes based on 3D printing technology. Three kinds of AAAM exhibited excellent workability and service performance, which laid a good foundation for studies on aggregate morphologies for asphalt mixture based on numerical simulation. Further, it could provide a scientific base for the replacement of natural aggregates in context of sustainable development of asphalt pavement and comparison to "standard aggregates" between different indoor and in-field tests. Particularly, it was of great significance for in-situ resource utilization of the Lunar and the Mars based on sintering technology, where these celestial bodies contained moderate amounts of SiO_2 estimated at 46.6%-47.1% and 9.3%-21.4%, and Al_2O_3 estimated at 43.4%-55% and7.2%-12.4%, respectively.

Acknowledgment

The authors sincerely appreciate the National Key Research and Development Program of China (NO. 2023YFB2603501).

References

Ambrosi, A., Pumera, M., 2016. 3D-printing technologies for electrochemical applications. Chemical society reviews 45(10), 2740-2755.

Andrzejuk, W., Barnat-Hunek, D., Siddique, R., Zegardło, B., Łagód, G., 2018. Application of recycled ceramic aggregates for the production of mineral-asphalt mixtures. Materials 11(5), 658.

Che, T., Pan, B., Ouyang, J., 2018. The laboratory evaluation of incorporating ceramsite into HMA as fine aggregates. Construction Building Materials 186, 1239-1246.

Chen, X., 2018. Preperation,Structure and Performance of Mullite Whisker Reinforced Ceramics-based Composites. [D].

Cho, S.-J., Jang, H.-N., Cho, S.-J., Yoon, Y.-S., Yoo, H.-M., 2023. Material recycling for manufacturing aggregates using melting slag of automobile shredder residues. Materials 16(7), 2664.

Deng, H., Deng, D., Du, Y., Lu, X., 2019. Using lightweight materials to enhance thermal resistance of asphalt mixture for cooling asphalt pavement. Advances in Civil Engineering 2019(1), 5216827.

Ding, X., Liu, F., Ma, T., Xiao, B., 2024. Effects of coarse aggregate morphology on Asphalt mixture's flowability: Parametric and prediction study. Case Studies in Construction Materials 21, e03735.

Gao, J., Wang, H., Bu, Y., You, Z., Hasan, M.R.M., Irfan, M., 2018. Effects of coarse aggregate angularity on the microstructure of asphalt mixture. Construction Building Materials 183, 472-484.

Goetz, W., Herrin, M., 1954. Effects of Aggregate Shape on the Stability of Bituminous Mixes.

Hu, J., Liu, P., Wang, D., Oeser, M., Canon Falla, G., 2019. Investigation on interface stripping damage at high-temperature using microstructural analysis. International Journal of Pavement Engineering 20(5), 544-556.

Jin, C., Wan, X., Liu, P., Yang, X., Oeser, M., 2021. Stability prediction for asphalt mixture based on evolutional characterization of aggregate skeleton. Computer‐Aided Civil Infrastructure Engineering 36(11), 1453-1466.

Kim, J.K., Kang, S.-S., Kim, H.G., Kwac, L.K., 2023. Mechanical properties and electromagnetic interference shielding of carbon composites with polycarbonate and acrylonitrile butadiene styrene resins. Polymers 15(4), 863.

Kusumawardani, D.M., Wong, Y.D., 2020. Evaluation of aggregate gradation on aggregate packing in porous asphalt mixture (PAM) by 3D numerical modelling and laboratory measurements. Construction Building Materials 246, 118414.

Lei, R., Yu, H., Qian, G., Zhang, C., Ge, J., Dai, W., 2024. Impact of aggregate morphology on the compression strength of asphalt mixtures during different compaction stages. Construction Building Materials 439, 137319.

Li, B., Zhang, C., Xiao, P., Wu, Z., 2019. Evaluation of coarse aggregate morphological characteristics affecting performance of heavy-duty asphalt pavements. Construction Building Materials 225, 170-181.

Li, W., Wang, D., Chen, B., Hua, K., Huang, Z., Xiong, C., Yu, H., 2022a. Preparation of artificial pavement coarse aggregate using 3D printing technology. Materials 15(4), 1575.

Li, W., Wang, D., Chen, B., Hua, K., Su, W., Xiong, C., Zhang, X., 2022b. Research on three-dimensional morphological characteristics evaluation method and processing quality of coarse aggregate, Buildings. p. 293.

Li, X., Shi, L., Liao, W., Wang, Y., Nie, W., 2024. Study on the influence of coarse aggregate morphology on the meso-mechanical properties of asphalt mixtures using discrete element method, Construction Building Materials. p. 136252.

Liu, P., Hu, J., Wang, D., Oeser, M., Alber, S., Ressel, W., Falla, G.C., 2017. Modelling and evaluation of aggregate morphology on asphalt compression behavior. Construction Building Materials 133, 196-208.

Liu, Y., Huang, Y., Sun, W., Nair, H., Lane, D.S., Wang, L., 2017. Effect of coarse aggregate morphology on the mechanical properties of stone matrix asphalt. Construction Building Materials 152, 48-56.

Liu, Y., Qian, Z., Zheng, D., 2023. Influence of coarse aggregate morphology on the mechanical characteristics of skeleton in porous asphalt concrete. International Journal of Pavement Engineering 24(1), 2252158.

Liu, Z., Huang, X., Sha, A., Wang, H., Chen, J., Li, C., 2019. Improvement of asphalt-aggregate adhesion using plant ash byproduct. Materials 12(4), 605.

Meier, W., 1988. Laboratory evaluation of shape and surface texture of fine aggregate for asphalt concrete. Transportation Research Record 1250, 25.

Min, Z., Yu, Z., Wang, Q., 2022. Behaviours of incorporating ceramsite into epoxy asphalt mixture as thermal resistance aggregates. International Journal of Pavement Engineering 23(9), 2954-2968.

Monismith, C., 1970. Influence of shape, size, and surface texture on the stiffness and fatigue response of asphalt mixtures. Highway Research Board Special Report(109).

Priyadharshini, P., Mohan, G., Santhi, A.S., 2012. A Review on Artificial Aggregates. International Journal of Earth Sciences and Engineering 05(974-5904).

Ramya, A., Vanapalli, S.L., 2016. 3D printing technologies in various applications. International Journal of Mechanical Engineering and Technology 7(3), 396-409.

Rodríguez-Fernández, I., Lastra-González, P., Indacoechea-Vega, I., Castro-Fresno, D., 2021. Technical feasibility for the replacement of high rates of natural aggregates in asphalt mixtures. International Journal of Pavement Engineering 22(8), 940-949.

Sahana, V., Thampi, G., 2018. 3D printing technology in industry, 2018 2nd International Conference on Inventive Systems and Control (ICISC). IEEE, pp. 528-533.

Shahrubudin, N., Lee, T.C., Ramlan, R., 2019. An overview on 3D printing technology: Technological, materials, and applications. Procedia manufacturing 35, 1286-1296.

Vila-Cortavitarte, M., Jato-Espino, D., Castro-Fresno, D., Calzada-Pérez, M., 2018. Self-healing capacity of asphalt mixtures including by-products both as aggregates and heating inductors. Materials 11(5), 800.

Wang, C., Fu, H., Fan, Z., Li, T., 2019. Utilization and properties of road thermal resistance aggregates into asphalt mixture. Construction Building Materials 208, 87-101.

Wang, D., Chen, G., Chen, Z., Tang, C., 2022. Study on preparation method of strength and morphology controlled aggregates used in asphalt mixture. Construction Building Materials 345, 128189.

Wang, H., Bu, Y., Wang, Y., Yang, X., You, Z., 2016. The Effect of Morphological Characteristic of Coarse Aggregates Measured with Fractal Dimension on Asphalt Mixture’s High-Temperature Performance. Advances in Materials Science Engineering 2016(1), 6264317.

Xie, X., Wang, D., Liu, D., Zhang, X., Oeser, M., 2016. Investigation of synthetic, self-sharpening aggregates to develop skid-resistant asphalt road surfaces. Wear 348, 52-60.

Xu, C., Wang, D., Zhang, S., Guo, E., Luo, H., Zhang, Z., Yu, H., 2021. Effect of lignin modifier on engineering performance of bituminous binder and mixture. Polymers 13(7), 1083.

Yan, Q., Dong, H., Su, J., Han, J., Song, B., Wei, Q., Shi, Y., 2018. A review of 3D printing technology for medical applications. Engineering 4(5), 729-742.

Yang, Y., Li, L., Zhao, J., 2019. Mechanical property modeling of photosensitive liquid resin in stereolithography additive manufacturing: Bridging degree of cure with tensile strength and hardness. Materials & Design 162, 418-428.

Yu, H., Zhu, Z., Leng, Z., Wu, C., Zhang, Z., Wang, D., Oeser, M., 2020. Effect of mixing sequence on asphalt mixtures containing waste tire rubber and warm mix surfactants. Journal of Cleaner Production 246, 119008.

Yu, H., Zhu, Z., Zhang, Z., Yu, J., Oeser, M., Wang, D., 2019. Recycling waste packaging tape into bituminous mixtures towards enhanced mechanical properties and environmental benefits. Journal of Cleaner Production 229, 22-31.

Yuan, J., He, P., Li, H., Xu, X., Sun, W., 2022. Preparation and Performance Analysis of

Ceramsite Asphalt Mixture with Phase-Change Material. Materials 15(17), 6021.

Zou, X., Xie, Y., Bi, Y., Li, B., Wang, W., Ye, X., 2023. Study on the shear strength of asphalt mixture by discrete element modeling with coarse aggregate morphology. Construction Building Materials 409, 134058.